J|A|C|S COMMUNICATIONS

Published on Web 06/29/2010

Rapid Acquisition of Multidimensional Solid-State NMR Spectra of Proteins Facilitated by Covalently Bound Paramagnetic Tags

Philippe S. Nadaud, Jonathan J. Helmus, Ishita Sengupta, and Christopher P. Jaroniec*

Department of Chemistry, The Ohio State University, Columbus, Ohio 43210

Received April 26, 2010; E-mail: jaroniec@chemistry.ohio-state.edu

Abstract: We describe a condensed data collection approach that facilitates rapid acquisition of multidimensional magic-angle spinning solid-state nuclear magnetic resonance (SSNMR) spectra of proteins by combining rapid sample spinning, optimized low-power radio frequency pulse schemes and covalently attached paramagnetic tags to enhance protein ^{1}H spin−lattice relaxation. Using EDTA-Cu^{2+}-modified K28C and N8C mutants of the B1 immunoglobulin binding domain of protein G as models, we demonstrate that high resolution and sensitivity 2D and 3D SSNMR chemical shift correlation spectra can be recorded in as little as several minutes and several hours, respectively, for samples containing ∼0.1−0.2 μmol of ^{13}C,^{15}N- or ^{2}H,^{13}C,^{15}N-labeled protein. This mode of data acquisition is naturally suited toward the structural SSNMR studies of paramagnetic proteins, for which the typical ^{1}H longitudinal relaxation time constants are inherently a factor of at least ∼3−4 lower relative to their diamagnetic counterparts. To illustrate this, we demonstrate the rapid site-specific determination of backbone amide ^{15}N longitudinal paramagnetic relaxation enhancements using a pseudo-3D SSNMR experiment based on ^{15}N−^{13}C correlation spectroscopy, and we show that such measurements yield valuable long-range ^{15}N−Cu^{2+} distance restraints which report on the three-dimensional protein fold.

Solid-state nuclear magnetic resonance (SSNMR) has recently emerged as a unique spectroscopic method, capable of providing atomic-resolution images of biological macromolecules that are not amenable to analysis by other high-resolution techniques.[1] It is well-known, however, that conventional SSNMR experiments employing moderate magic-angle spinning (MAS) rates (∼10−25 kHz) and high radio frequency (RF) ^{1}H decoupling fields generally suffer from inherently low sensitivity. This stems, in part, from the fact that most of the total experiment time is occupied by ∼2−3 s recycle delays between successive scans, required to restore the equilibrium ^{1}H magnetization for cross-polarization[2] and minimize RF sample heating and probe duty cycle. One general approach toward reducing interscan delays and enhancing the sensitivity of SSNMR experiments involves the introduction of paramagnetic species into the sample of interest.[3] Such paramagnetic dopants promote rapid longitudinal relaxation of the nearby ^{1}H spins and this effect is transferred to other protons via efficient ^{1}H−^{1}H spin diffusion,[4] the end result being that all ^{1}H nuclei return to equilibrium with an effective longitudinal relaxation time constant (T_1), which is considerably less than that for an undoped diamagnetic sample.

Recently, Ishii and co-workers have introduced a paramagnetic relaxation-assisted condensed data collection (PACC) method for increasing the sensitivity of SSNMR spectra of biomolecules,[5] which combines paramagnetic doping,[3] rapid MAS ($\nu_r \geq$ ∼40 kHz) and low-power RF pulse schemes,[6] and short recycle delays (∼0.2−0.3 s). This approach considerably accelerates SSNMR data acquisition and has enabled the analysis of nanomolar quantities of ^{13}C,^{15}N-labeled proteins. The paramagnetic dopant in this case is an aqueous Cu(II)-EDTA (or Ni(II)-EDTA) complex, diffused into a hydrated protein SSNMR sample, and the proposed ^{1}H T_1 relaxation enhancement mechanism involves Cu(II)-EDTA in the solution phase making transient contacts with protein molecules immobilized in microcrystals or other ordered assemblies. These transient contacts lead to rapid relaxation by Cu^{2+} ions of the protein ^{1}H nuclei at the solid−liquid interface, followed by spin diffusion to equalize the ^{1}H longitudinal relaxation rates throughout the immobilized protein sample.[5] The PACC approach has been extended to studies of highly deuterated proteins,[7] and analogous fast recycling SSNMR experiments have been reported for native metalloproteins.[8] The use of Cu(II)-chelating lipids to enhance the sensitivity of SSNMR spectra of membrane-associated peptides has also been demonstrated very recently.[9]

We have recently shown that long-range, up to ∼20 Å, electron−nucleus distance restraints can be obtained using MAS SSNMR techniques in ^{13}C,^{15}N-labeled proteins modified with covalently attached paramagnetic tags, including nitroxide spin labels[10] and transition metal−EDTA complexes.[11] Here we show that such proteins, which inherently display ∼3−4-fold reduced ^{1}H T_1 times relative to their diamagnetic counterparts, are ideally suited for application of PACC-type condensed data acquisition schemes and permit high resolution and sensitivity 2D and 3D SSNMR spectra to be recorded within several minutes to several hours for samples containing ∼0.1−0.2 μmol of labeled protein. Most importantly, this accelerated mode of data collection enables the rapid determination of site-specific nuclear paramagnetic relaxation enhancements (PREs), which yield valuable long-range information about the three-dimensional protein fold.

The experiments are demonstrated on EDTA-Cu^{2+}-modified N8C and K28C mutants of the B1 immunoglobulin binding domain of protein G (GB1), referred to as 8EDTA-Cu^{2+} and 28EDTA-Cu^{2+} for brevity, but note that similar data were obtained for four other EDTA-Cu^{2+} GB1 variants. Protein microcrystals for SSNMR were prepared by precipitating ∼1 mg (∼150 nmol) of ^{13}C,^{15}N (CN) or ^{2}H,^{13}C,^{15}N (DCN) labeled EDTA-Cu^{2+} proteins with unlabeled wild-type GB1 in an ∼1:3 molar ratio[11] (see Supporting Information). At 40 kHz MAS, the ^{1}H T_1 times of CN- and DCN-EDTA-Cu^{2+} proteins were determined by standard inversion−recovery methods to be ∼120 ms (data not shown), while the ^{1}H T_1's of corresponding diamagnetic EDTA-Zn^{2+} samples were ∼450 ms.

In Figure 1 we show representative 2D and 3D chemical shift correlation spectra of DCN-28EDTA-Cu^{2+} acquired at 40 kHz MAS using optimized low-power pulse schemes (Figures S1 and S2). The 2D NCO spectrum (Figure 1A), which was recorded in only ∼7 min (note that this could be reduced further with only a modest decrease in sensitivity or, alternatively, slightly higher sensitivity could be achieved within the same experiment time by using shorter recycle delays, ∼1.2−1.5 × instead of 3 × ^{1}H T_1), exhibits particularly high digital resolution due to the use of a spin-state selective (S^3E) filter to suppress ^{13}CO−^{13}Cα J-couplings during detection[12] and relatively long evolution times in t_1 and t_2. We note here that signals arising from all backbone amide ^{15}N's, including residues in the vicinity of the paramagnetic center (located ∼10 Å away from the Cu^{2+} ion[11]), are readily detected in this spectrum; the cross-peak signal-to-noise (S/N)

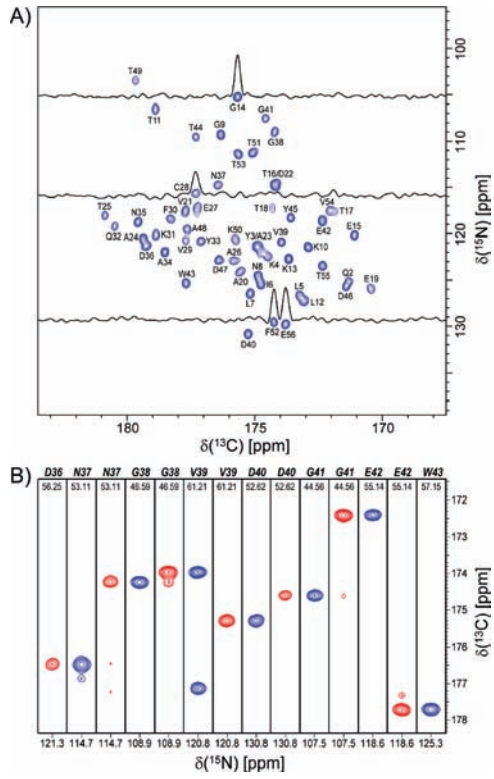

Figure 1. Solid-state NMR spectra of $^{2}H,^{13}C,^{15}N$-labeled 28EDTA-Cu^{2+} (~150 nmol protein) back-exchanged with H_2O, recorded at 11.7 T and 40 kHz MAS. (A) 2D $^{15}N-^{13}CO$ (NCO) spectrum recorded using the 2D NCO-S^3E pulse scheme[12] (Figure S1A). The spectrum was acquired in ~7 min with 2 scans per row, 0.36 s recycle delay ($3 \times {}^{1}H\ T_1$), $t_{1,max}(^{15}N) = 25.6$ ms, and $t_{2,max}(^{13}C) = 30$ ms and processed with 81°-shifted sine-bell window functions in F_1 and F_2. (B) Representative strips from 3D $^{15}N-^{13}C\alpha-^{13}CO$ (NCACO; red contours) and $^{13}C\alpha-^{15}N-^{13}CO$ spectra (CANCO; blue contours) showing sequential backbone assignments for residues D36-W43, recorded using the pulse schemes in Figure S2. Each spectrum was acquired in ~2.9 h with 2 scans per row, 0.36 s recycle delay, $t_{1,max}(^{15}N) = 18.4$ ms, $t_{2,max}(^{13}C) = 8$ ms, and $t_{3,max}(^{13}C) = 30$ ms and processed with 81°-shifted sine-bell window functions in each dimension.

ratios range from 12 (T18N-T17CO) to 38 (K13N-L12CO) and the average *S/N* ratio was found to be 27 ± 6. Most importantly, a comparable 2D NCO spectrum, displaying signal intensities only ~25% lower on average, could be obtained for the fully protonated CN-28EDTA-Cu^{2+} sample in the same amount of time (Figure S4). Small regions from 3D CANCO and NCACO spectra recorded in ~2.9 h each, which enable complete sequential ^{15}N, ^{13}CO, and $^{13}C\alpha$ resonance assignments to be established for DCN-28EDTA-Cu^{2+}, are shown in Figure 1B, and additional data sets including 2D N(CA)CO and 3D CANCO, NCACO, and NCACB are shown in Figures S5−S7 for DCN- and CN-28EDTA-Cu^{2+}. Altogether, these data indicate that while a high degree of protein deuteration facilitates efficient ^{1}H decoupling and results in highest sensitivity spectra, it is not absolutely essential. Indeed, in most cases (3D NCACB being the main exception) 2D and 3D spectra of comparable quality could be recorded in approximately the same amount of time for the fully protonated protein, and as expected, deuteration afforded the largest sensitivity gains for correlations involving $^{13}CH_2$ groups (glycine Cα and most Cβ).

The ability to rapidly record high-quality 2D and 3D spectra of paramagnetic proteins has major practical consequences for protein structural studies based on SSNMR measurements of paramagnetic relaxation enhancements[10,11] and pseudocontact shifts.[13] To illustrate this, in Figure 2 we show site-specific measurements of backbone amide ^{15}N longitudinal relaxation rates[11,14] ($^{15}N\ R_1$) for DCN-28EDTA-Cu^{2+} and CN-8EDTA-Cu^{2+}. A comparison of $^{15}N\ R_1$ data for DCN-28EDTA-Cu^{2+} and CN-28EDTA-Cu^{2+} (Figure S8) reveals

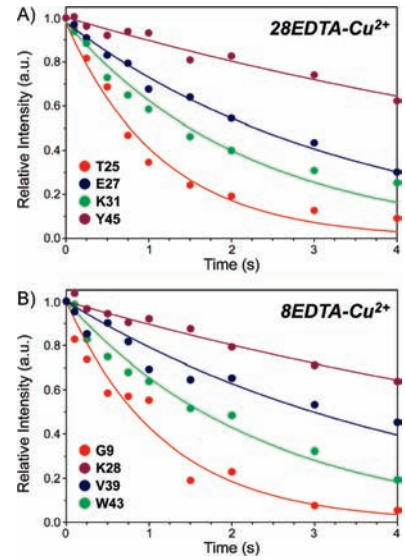

Figure 2. (A) Representative SSNMR measurements of backbone amide ^{15}N longitudinal relaxation rates, $R_1 = T_1^{-1}$, for residues T25, E27, K31, and Y45 in DCN-28EDTA-Cu^{2+}. Decaying single exponential fits are shown as solid lines. Spectra were recorded at 11.7 T and 40 kHz MAS using the pulse scheme in Figure S3. The experiment time was ~10 h. (B) Same as panel (A) for G9, K28, V39, and W43 in CN-8EDTA-Cu^{2+}.

that protein deuteration has a negligible effect on the measured longitudinal relaxation rates. The pseudo-3D SSNMR experiments, which consisted of a series of ten 2D NCO spectra with increasing ^{15}N longitudinal relaxation delays up to 4 s, could be recorded in as little as ~10 h per protein sample. Remarkably, previous measurements of this type performed using conventional SSNMR schemes at ~11 kHz MAS, which utilized ~7−8 times as much labeled protein and contained fewer points in the ^{15}N relaxation dimension, required ~2−4 days of measurement time to achieve comparable results.[11] The significant dispersion in the measured backbone amide $^{15}N\ R_1$ rates is primarily related to the proximity of the ^{15}N nuclei to the Cu^{2+} ion. For instance, while for 28EDTA-Cu^{2+} the α-helical amino acid residues, A24-Q32, display significantly elevated relaxation rates (cf., Figures 2A and S8A), they are among the slowest relaxing amino acids in 8EDTA-Cu^{2+} as illustrated by the relaxation trajectory for K28 in Figure 2B. In contrast, for 8EDTA-Cu^{2+} the largest relaxation rates are found for residues located in strands $\beta1-\beta4$, in proximity to the Cu^{2+} center.

To quantitatively assess the paramagnetic contributions to ^{15}N longitudinal relaxation rates due to the presence of Cu^{2+} ions, analogous relaxation trajectories were recorded for the corresponding diamagnetic control samples, DCN-28EDTA-Zn^{2+} and CN-8EDTA-Zn^{2+} (representative trajectories are shown in Figures S10 and S11). For each residue the longitudinal ^{15}N paramagnetic relaxation enhancement (Γ_1^N) is obtained by taking the difference between the $^{15}N\ R_1$ values for EDTA-Cu^{2+} and EDTA-Zn^{2+} proteins, found by modeling the relaxation trajectories as single exponential decays. Figure 3 shows the ^{15}N longitudinal PREs for 28EDTA-Cu^{2+} and 8EDTA-Cu^{2+} as a function of residue number and location within the three-dimensional protein structure. The observed Γ_1^N values range between ~0.03 and 0.8 s^{-1}, and as expected, the PRE magnitudes are highly correlated with the $^{15}N-Cu^{2+}$ separation. Additionally, the residue-specific ^{15}N PRE measurements permit distances between the Cu^{2+} ion and backbone amide ^{15}N nuclei to be estimated as described previously[11] by using the Solomon−Bloembergen equation[15] (cf., Tables S1 and S2).

To evaluate the potential of the measured ^{15}N PREs and $^{15}N-Cu^{2+}$ distances to yield useful structural information, in Figure 4A we show the comparison of the experimentally observed Γ_1^N values and the corresponding values calculated from structural models of 8EDTA-

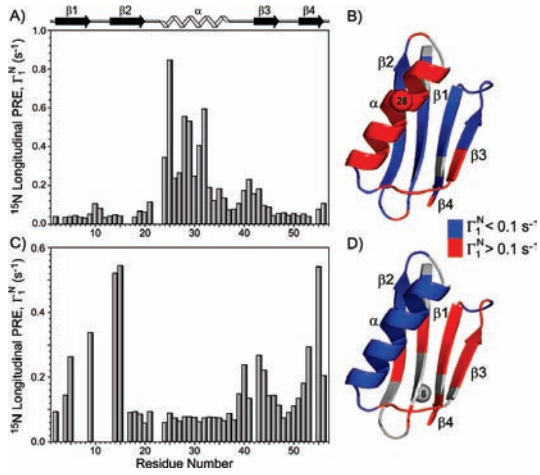

Figure 3. (A) Backbone amide ^{15}N longitudinal paramagnetic relaxation enhancements, $\Gamma_1^N = R_1(Cu^{2+}) - R_1(Zn^{2+})$, for DCN-28EDTA-$Cu^{2+}$ as a function of residue number. Γ_1^N was set to zero for residues where quantitative measurement was not possible due to insufficient spectral resolution. (B) Ribbon diagram of GB1 (PDB entry 1PGA) with Γ_1^N values mapped onto the structure. Residues with $\Gamma_1^N < 0.1$ s^{-1} (corresponding to ^{15}N−Cu^{2+} distances, $r_{N-Cu} > \sim 15$ Å) and $\Gamma_1^N > 0.1$ s^{-1} ($r_{N-Cu} < \sim 15$ Å) are highlighted in blue and red, respectively, and residues for which Γ_1^N was not determined are colored in gray. The residue containing the EDTA-Cu^{2+} side chain is indicated by a sphere. (C,D) Same as panels (A,B) for CN-8EDTA-Cu^{2+}.

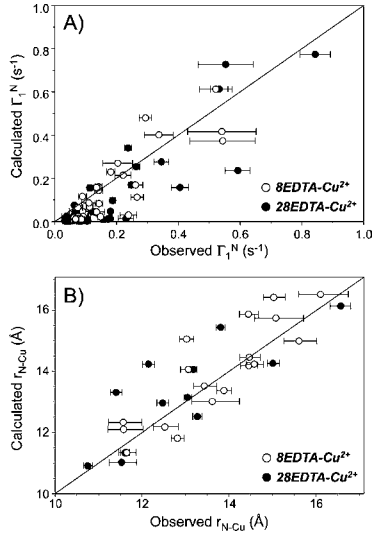

Figure 4. Comparison between the experimentally determined (A) ^{15}N longitudinal PREs and (B) ^{15}N−Cu^{2+} distances, and corresponding values calculated from structural models of 8EDTA-Cu^{2+} and 28EDTA-Cu^{2+}.

Cu^{2+} and 28EDTA-Cu^{2+}, constructed based on the atomic coordinates of wild-type GB1 using Xplor-NIH.[16] Overall, the experimental PREs are found to be in good agreement with those predicted from the protein structural models, with a root-mean-squared (rms) deviation of ∼0.09 s^{-1}. The largest deviations are seen for a cluster of measurements corresponding to the smallest calculated Γ_1^N values ($\Gamma_1^N < 0.05$ s^{-1}, associated with the longest ^{15}N−Cu^{2+} distances, $r_{N-Cu} > 17$ Å), where the experimentally observed PREs systematically exceed those predicted by the protein structural models. As discussed previously,[11] these systematic deviations most likely reflect contributions from residual intermolecular ^{15}N−Cu^{2+} couplings due to insufficient dilution of EDTA-Cu^{2+} proteins in the diamagnetic matrix. In contrast, the agreement between the observed and expected ^{15}N PREs, and, especially, ^{15}N−Cu^{2+} distances (note that for the larger PRE values, the PRE is a highly sensitive function of the ^{15}N−Cu^{2+} distance; e.g., PREs of 0.2 and 0.6 correspond to distances of ca. 13.5 and 11.5 Å, respectively), is substantially improved for measurements corresponding to Γ_1^N calculated > 0.05 s^{-1}. Figure 4B shows a set of ∼30 distance measurements in 8EDTA-Cu^{2+} and 28EDTA-Cu^{2+} that fall into this category. These data reveal a strong correlation between the measured and predicted ^{15}N−Cu^{2+} distances, with an rms deviation of ∼0.9 Å, indicating that such distance restraints can be suitable for applications to SSNMR protein structure refinement.

In conclusion, we have demonstrated that a condensed data acquisition approach[5] that uses covalently bound paramagnetic tags to enhance ^{1}H spin−lattice relaxation facilitates acquisition of high resolution and sensitivity MAS SSNMR spectra in as little as several minutes for protein samples containing only ∼0.1−0.2 μmol of ^{13}C,^{15}N- or ^{2}H,^{13}C,^{15}N-labeled protein. Most significantly, this mode of data collection is naturally suited toward structural SSNMR studies of paramagnetic proteins based on measurements of pseudocontact shifts and nuclear PREs,[10,11,13] as illustrated here for two paramagnetic mutants of protein GB1. In addition, the possibility of being able to modulate protein ^{1}H T_1 times by directly embedding regularly spaced paramagnetic moieties at specific sites in the protein lattice promises to be a generally applicable tool for enhancing the sensitivity of MAS NMR spectra of natively diamagnetic proteins found in a variety of environments, which may pose challenges for traditional PACC schemes based on external paramagnetic doping,[5,7] including large supramolecular aggregates and biological membranes.

Acknowledgment. This work was supported by the National Science Foundation (CAREER Award MCB-0745754 to C.P.J.). We thank Dr. Charles Schwieters for assistance with Xplor-NIH.

Supporting Information Available: Experimental section, pulse scheme diagrams, additional NMR spectra, relaxation trajectories, and tables. This material is available free of charge via the Internet at http://pubs.acs.org.

References

(1) McDermott, A. *Annu. Rev. Biophys.* **2009**, *38*, 385–403. Lange, A.; Giller, K.; Hornig, S.; Martin-Eauclaire, M. F.; Pongs, O.; Becker, S.; Baldus, M. *Nature* **2006**, *440*, 959–962. Wasmer, C.; Lange, A.; Van Melckebeke, H.; Siemer, A. B.; Riek, R.; Meier, B. H. *Science* **2008**, *319*, 1523–1526. Helmus, J. J.; Surewicz, K.; Nadaud, P. S.; Surewicz, W. K.; Jaroniec, C. P. *Proc. Natl. Acad. Sci. U.S.A.* **2008**, *105*, 6284–6289.
(2) Pines, A.; Gibby, M. G.; Waugh, J. S. *J. Chem. Phys.* **1973**, *59*, 569–590.
(3) Ganapathy, S.; Naito, A.; McDowell, C. A. *J. Am. Chem. Soc.* **1981**, *103*, 6011–6015.
(4) Bloembergen, N. *Physica* **1949**, *15*, 386–426.
(5) Wickramasinghe, N. P.; Kotecha, M.; Samoson, A.; Past, J.; Ishii, Y. *J. Magn. Reson.* **2007**, *184*, 350–356. Wickramasinghe, N. P.; Parthasarathy, S.; Jones, C. R.; Bhardwaj, C.; Long, F.; Kotecha, M.; Mehboob, S.; Fung, L. W. M.; Past, J.; Samoson, A.; Ishii, Y. *Nat. Methods* **2009**, *6*, 215–218.
(6) Ernst, M.; Meier, M. A.; Tuherm, T.; Samoson, A.; Meier, B. H. *J. Am. Chem. Soc.* **2004**, *126*, 4764–4765. Vijayan, V.; Demers, J. P.; Biernat, J.; Mandelkow, E.; Becker, S.; Lange, A. *ChemPhysChem* **2009**, *10*, 2205–2208.
(7) Linser, R.; Chevelkov, V.; Diehl, A.; Reif, B. *J. Magn. Reson.* **2007**, *189*, 209–216.
(8) Laage, S.; Sachleben, J. R.; Steuernagel, S.; Pierattelli, R.; Pintacuda, G.; Emsley, L. *J. Magn. Reson.* **2009**, *196*, 133–141. Bertini, I.; Emsley, L.; Lelli, M.; Luchinat, C.; Mao, J.; Pintacuda, G. *J. Am. Chem. Soc.* **2010**, *132*, 5558–5559.
(9) Yamamoto, K.; Xu, J.; Kawulka, K. E.; Vederas, J. C.; Ramamoorthy, A. *J. Am. Chem. Soc.* **2010**, *132*, 6929–6931.
(10) Nadaud, P. S.; Helmus, J. J.; Hofer, N.; Jaroniec, C. P. *J. Am. Chem. Soc.* **2007**, *129*, 7502–7503.
(11) Nadaud, P. S.; Helmus, J. J.; Kall, S. L.; Jaroniec, C. P. *J. Am. Chem. Soc.* **2009**, *131*, 8108–8120.
(12) Laage, S.; Lesage, A.; Emsley, L.; Bertini, I.; Felli, I. C.; Pierattelli, R.; Pintacuda, G. *J. Am. Chem. Soc.* **2009**, *131*, 10816–10817.
(13) Balayssac, S.; Bertini, I.; Lelli, M.; Luchinat, C.; Maletta, M. *J. Am. Chem. Soc.* **2007**, *129*, 2218–2219. Balayssac, S.; Bertini, I.; Bhaumik, A.; Lelli, M.; Luchinat, C. *Proc. Natl. Acad. Sci. U.S.A.* **2008**, *105*, 17284–17289.
(14) Giraud, N.; Bockmann, A.; Lesage, A.; Penin, F.; Blackledge, M.; Emsley, L. *J. Am. Chem. Soc.* **2004**, *126*, 11422–11423.
(15) Solomon, I. *Phys. Rev.* **1955**, *99*, 559–565. Bloembergen, N.; Morgan, L. O. *J. Chem. Phys.* **1961**, *34*, 842–850.
(16) Schwieters, C. D.; Kuszewski, J. J.; Tjandra, N.; Clore, G. M. *J. Magn. Reson.* **2003**, *160*, 65–73.

JA103545E